Journal Pre-proofs

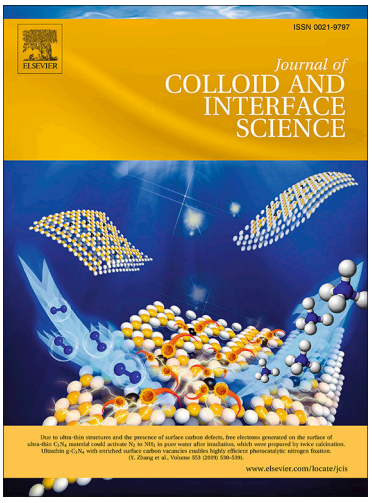

Regular Article

Ultrafast joule-heating-assisted O, N dual-doping of unfunctionalized carbon enhances Ru nanoparticle-catalyzed hydrogen production

Yihan Zhang, Song Wu, Ting Sun, Qianggen Li, Guangyin Fan

PII: S0021-9797(24)02717-6
DOI: https://doi.org/10.1016/j.jcis.2024.11.141
Reference: YJCIS 36353

To appear in: *Journal of Colloid and Interface Science*

Received Date: 14 September 2024
Revised Date: 14 November 2024
Accepted Date: 18 November 2024

Please cite this article as: Y. Zhang, S. Wu, T. Sun, Q. Li, G. Fan, Ultrafast joule-heating-assisted O, N dual-doping of unfunctionalized carbon enhances Ru nanoparticle-catalyzed hydrogen production, *Journal of Colloid and Interface Science* (2024), doi: https://doi.org/10.1016/j.jcis.2024.11.141

Ultrafast joule-heating-assisted O, N dual-doping of unfunctionalized carbon enhances Ru nanoparticle-catalyzed hydrogen production

Yihan Zhang, Song Wu, Ting Sun, Qianggen Li* and Guangyin Fan*

College of Chemistry and Materials Science, Sichuan Normal University, Chengdu 610068, China

* Corresponding author

Emails: liqgen@sicnu.edu.cn (Q. Li); fanguangyin@sicnu.edu.cn (G. Fan)

Abstract: The development of a rapid and convenient strategy to regulate the surface microenvironment of inert carbon supports, along with the physicochemical properties of their supported metal nanoparticles, is essential for enhancing catalytic performance. In this study, we describe a straightforward and efficient solid-state microwave method that utilizes a household microwave oven to achieve the co-doping of oxygen and nitrogen in unfunctionalized carbon black (ONCB) using urea as a nitrogen source. The microwave solid-state treatment of commercial carbon black (CB) with urea not only introduces a significant number of heteroatomic functional groups but also substantially increases the pore size and pore volume of the matrix. These enhancements facilitate the uniform growth and dispersion of ultrafine Ru nanoparticles on the surface of ONCB. Consequently, the Ru/ONCB catalyst provides abundant catalytic active sites and mass transfer channels, thereby improving catalytic performance for hydrogen evolution from ammonia borane hydrolysis (ABH). The turnover frequency of Ru/ONCB for ABH reaches 4529 ± 238 min^{-1} (determined based on Ru dispersion), surpassing a range of analogues and many previously reported carbon-supported Ru catalysts. This study presents a simple and rapid strategy to regulate the surface microenvironment of unfunctionalized carbon support, thereby enhancing the catalytic performance of its supported metal nanoparticles for catalytic hydrogen generation.

Keywords: Ruthenium nanoparticles; microwave-assisted solid strategy; surface microenvironment engineering; ammonia borane hydrolysis; hydrogen generation

1. Introduction

The extensive consumption of fossil fuels has led to environmental issues such as the greenhouse effect, acid rain, and dust pollution, which have had a global impact on industrial production [1]. Consequently, there is a pressing need to explore high-energy, pollution-free, and sustainable clean energy sources to replace fossil fuels [2, 3]. Hydrogen is regarded as an ideal alternative fuel due to its cleanliness, non-polluting nature, and sustainability [4-7]. However, the large-scale application of hydrogen faces significant challenges, particularly in relation to hydrogen compression and liquefaction. Recent studies have concentrated on hydrogen generation through electrocatalytic hydrogen evolution reactions, photocatalytic hydrogen evolution, and the dehydrogenation of hydrogen storage materials for potential practical application [8]. Notably, hydrogen generation from hydrogen storage materials has attracted increasing attention. Among various hydrogen storage materials, ammonia borane (AB) stands out due to its high hydrogen content, superior stability, and excellent solubility [9-12]. Furthermore, AB can release hydrogen through thermal decomposition or hydrolysis, with catalytic hydrolysis of AB being considered a particularly promising method. The hydrolysis of AB (ABH) can occur even under ambient conditions with the presence of a suitable catalyst [13].

To accelerate hydrogen release, various noble metal catalysts, including Pt, Pd, Rh, and Ru, have been extensively studied [14-29]. Among these precious metals, Ru is particularly attractive due to its relatively low cost and abundance [30-37]. However, a significant challenge faced by metal nanoparticles (NPs) is their tendency to

agglomerate, which adversely affects the stability and activity of the catalysts. Generally, the selection of appropriate support materials can mitigate aggregation and facilitate the formation of ultrasmall metal NPs [38-40]. Previous literature indicates that carbon materials, such as activated carbon [41, 42], graphene [43], and carbon nanotubes [44], are commonly used as carrier materials due to their large specific surface areas, low cost, and stability. Furthermore, heteroatom-doped carbon materials (e.g., N, O, S, and P) have been shown to effectively immobilize metal NPs on the carbon skeletons and control their size [45]. Among these dopants, N and O have attracted considerable attention due to their excellent stabilization roles in regulating the geometric and electronic structures of metal NPs [46]. Notably, the co-doping of supporting materials with N and O can provide synergistic effects that enhance the catalytic performance of active metal sites. Typically, N/O doping can be achieved through two strategies: acid or base activation [47] and high-temperature pyrolysis [48]. While the former approach can partially modify carbon materials, it has several drawbacks, including the high consumption of acids and alkalis and the potential emission of toxic gases during the treatment processes. The latter method involves selecting suitable nitrogen-containing carbon source materials as precursors and subjecting them to pyrolytic carbonization. Although this method is commonly employed for treating carbon materials, determining the optimal atmosphere and temperature remains a challenge. Therefore, developing a fast and convenient method for preparing O/N co-doped porous carbon materials to stabilize Ru NPs for hydrogen evolution from ABH is of significant scientific importance.

In this study, O/N co-doped commercial conductive carbon (ONCB) was synthesized using urea as a nitrogen source in a household microwave oven, employing a rapid 40-second microwaving process. This microwave-assisted strategy not only introduced abundant O and N functional groups but also generated numerous defects and a porous structure. These characteristics help to mitigate the overgrowth of ultrafine Ru NPs and foster strong electron interactions between Ru NPs and ONCB, contributing to the excellent catalytic activity of Ru/ONCB. With a Ru loading of 1.2 wt%, Ru/ONCB demonstrated the highest catalytic activity for ABH, achieving a turnover frequency (TOF) of 4529 ± 238 min^{-1} (determined based on Ru dispersion) at room temperature, thus surpassing other reported Ru-based catalysts (Table S3). The reaction kinetics for hydrogen evolution from ABH over Ru/ONCB were studied under different parameters, including catalyst dosage, substrate concentration and reaction temperature. Furthermore, the reusability of Ru/ONCB was assessed through five consecutive ABH reactions. The rate-determining step (RDS) for hydrogen production from ABH was investigated using isotope experiments. This work highlights the advantages of microwave-assisted solid-state synthesis of heteroatom-doped porous carbon materials for anchoring ultrafine metal NPs and achieving efficient catalysis of ABH for hydrogen production.

2. Experimental section

2.1. Chemicals and materials

$RuCl_3 \cdot nH_2O$ (containing 35.0 wt% of Ru), urea (AR), deuteroxide (D_2O, AR), ammonia borane, commercial carbon black, and sodium citrate (≥ 99.0%) were

purchased from Aladdin Industrial Inc. China. Sodium hypochlorite solution (NaClO, 4.0%) was purchased from Macklin Co. Sodium nitroprusside ($Na_2[Fe(CN)_5NO]\cdot 2H_2O$, ≥ 98.0%) was purchased from Alfa Aesar Co. Ammonium chloride (NH_4Cl, ≥ 99.5%), salicylic acid (≥ 99.5%), and sodium hydroxide (NaOH, ≥ 98.0%) were purchased from Chengdu Chron Chemicals Co. All chemicals were used directly without any further purification. Deionized water was used for all experimental tests.

2.2. Characterization

The morphology was analyzed using transmission electron microscopy (TEM) measurement conducted on a JEOL model 2010 instrument, which operated at an accelerating voltage of 200 kV, alongside a high qualitative scanning electron microscopy (SEM, PEI/Quanta250). Powder X-ray diffraction (XRD) patterns were recorded on a Rigaku X-ray diffractometer D/max-2200/PC equipped with Cu Kα radiation (40 kV, 20 mA). The samples were scanned at a rate of 0.02 $step^{-1}$ over the range of 10–80°. The Brunauer−Emmett−Teller (BET) specific surface areas of the samples were determined from the N_2 adsorption/desorption isotherm at liquid nitrogen temperature using a Micromeritics TriStar II instrument. Surface electronic states were characterized using X-ray photoelectron spectroscopy (XPS, Kratos XSAM800). The Raman spectra of the samples were recorded on a HORIBAJ system. The metal loadings of the catalysts were measured via inductively coupled plasma optical emission spectrometry (ICP-OES, PerkinElmer Optima 8000 equipment).

2.3. Preparation of ONCB and Ru/ONCB

A mixture of commercial carbon black (CB, 0.2 g) and urea (0.1 g) was added to a

100 mL beaker containing 20 mL of anhydrous ethanol. The mixture underwent ultrasonication for 20 min to achieve a uniform suspension. Subsequently, the suspension was stirred in a water bath at 80 °C until the solvent was completely evaporated. The resulting solid was then placed in a vacuum oven at 100 °C for 10 h. Following this, 0.1 g of the prepared powder was transferred to a quartz glass bottle, which was sealed and subjected to heating treatment in a microwave reactor at 1000 W for durations of 20 s, 30 s, 40 s, and 50 s. Finally, the treated carbon materials were washed with 100 mL of water to remove impurities. The resulting products were dried at 100 °C for 10 h, and the obtained black powders were designated as ONCB-20, ONCB-30, ONCB-40 (collectively abbreviated as ONCB), and ONCB-50, respectively. Furthermore, a control sample, which involved treating CB with 40-second microwave radiation, was named OCB.

To prepare Ru/ONCB, 10 mg of ONCB and the desired amounts of $RuCl_3 \cdot nH_2O$ were dissolved in a 25 mL flask containing 4 mL of water. The resulting suspension was subjected to ultrasonic treatment to ensure the uniform dispersion of Ru^{3+} ions and ONCB. Subsequently, 1.0 mL of an aqueous AB solution (1.0 M) was injected into the flask under magnetic stirring to reduce Ru^{3+} ions and achieve a consistent distribution of Ru NPs on the ONCB surface. Upon completion of the reduction process, the suspension was processed through centrifugation, followed by washing with 100 mL of water to remove impurities from the catalyst surface. The sample was the subjected to vacuum drying at 80 °C for 24 h. The Ru loadings of the Ru/ONCB catalysts were determined by ICP-OES to be 0.4, 0.8, 1.2, and 1.6 wt%. Additionally, control samples

of Ru/ONCB-20, Ru/ONCB-30, Ru/ONCB-50, Ru/CB, and Ru/OCB, each with the same Ru loading as Ru/ONCB, were synthesized under identical protocols using ONCB-20, ONCB-30, ONCB-50, CB, and OCB as the supports.

2.4. Catalytic hydrolysis of AB

Typically, 10.0 mg of Ru/ONCB catalyst was added to a double-necked flask containing 4.0 mL of water. The mixture was ultrasonicated to create a uniformly dispersed suspension. Subsequently, 1.0 mL of AB solution (1.0 M) was injected into the flask to initiate the hydrolysis reaction. The volume of hydrogen released was measured using the drainage method, while the time was simultaneously recorded with a stopwatch. To investigate the chemical kinetics of ABH, control experiments were conducted, starting with 5.0 mL of AB solution (200 mM) at varying Ru concentrations (0.3, 0.6, 0.9, and 1.2 mM). Additionally, to examine the effects of AB dosages on catalytic ABH, control experiments were performed using 10.0 mg of Ru/ONCB (1.2 wt% Ru) and 5.0 mL of AB solution at various concentrations (100, 200, 300, and 400 mM) at 25 °C. To determine the activation energy (Ea) for ABH, reactions were conducted with 10.0 mg of Ru/ONCB (1.2 wt% Ru) and 5.0 mL of AB solution (200 mM) at different reaction temperatures (20, 25, 30, and 35 °C). An isotopic kinetic experiment was also carried out by replacing water with D_2O while maintaining all other conditions unchanged. The impact of NaOH dosages on ABH over Ru/ONCB was investigated by adding specific amounts of NaOH (0.30-0.75 g) without altering other reaction conditions.

2.5. Reusability of Ru/ONCB for ABH

The reusability of the Ru/ONCB catalyst for ABH was investigated using 10 mg of Ru/ONCB (1.2 wt% Ru) in conjunction with 5 mL of 200 mM AB solution, which composed of 1.0 mL of AB (1.0 M) and 4.0 mL of water) at 25 °C. After each cycle, the catalyst was recovered and reused in the subsequent run with 4.0 mL of fresh water and 1.0 mL of AB solution (1.0 M). The reusability test was repeated five times, and the recovered catalyst (named as r-Ru/ONCB) was subjected to characterization.

2.6. Calculation

The TOF value was calculated using the method previously reported in the literature (Eq. 1) [49]:

$$\mathrm{TOF} = \frac{\mathrm{P_{atm}V_{H_2}/RT}}{\mathrm{n_{Ru}\ t}} \quad \text{(Eq.1)}$$

where P_{atm} is the atmospheric pressure (101325 Pa), V_{H_2} is the volume of generated hydrogen at a conversion of 50%, R is the ideal gas constant (8.314 J $mol^{-1}\cdot K^{-1}$), T is the reaction temperature (K), n_{Ru} is the total number of moles of Ru atoms in the catalyst, and t is the reaction time. The corresponding TOF values were further calculated based on the Ru dispersion determined by H_2-TPD measurements.

3. Results and discussion

The preparation process for the Ru/ONCB catalyst is illustrated in Fig. 1. The ONCB, a porous carbon doped with oxygen and nitrogen, was synthesized by mixing CB and urea in a microwave oven reactor, followed by a short-time microwave irradiation. Subsequently, Ru NPs were deposited onto the ONCB matrix to facilitate efficient hydrogen production through ABH. TEM was utilized to determine the morphology and microstructure of CB, ONCB, Ru/CB, and Ru/ONCB. The CB and ONCB matrices

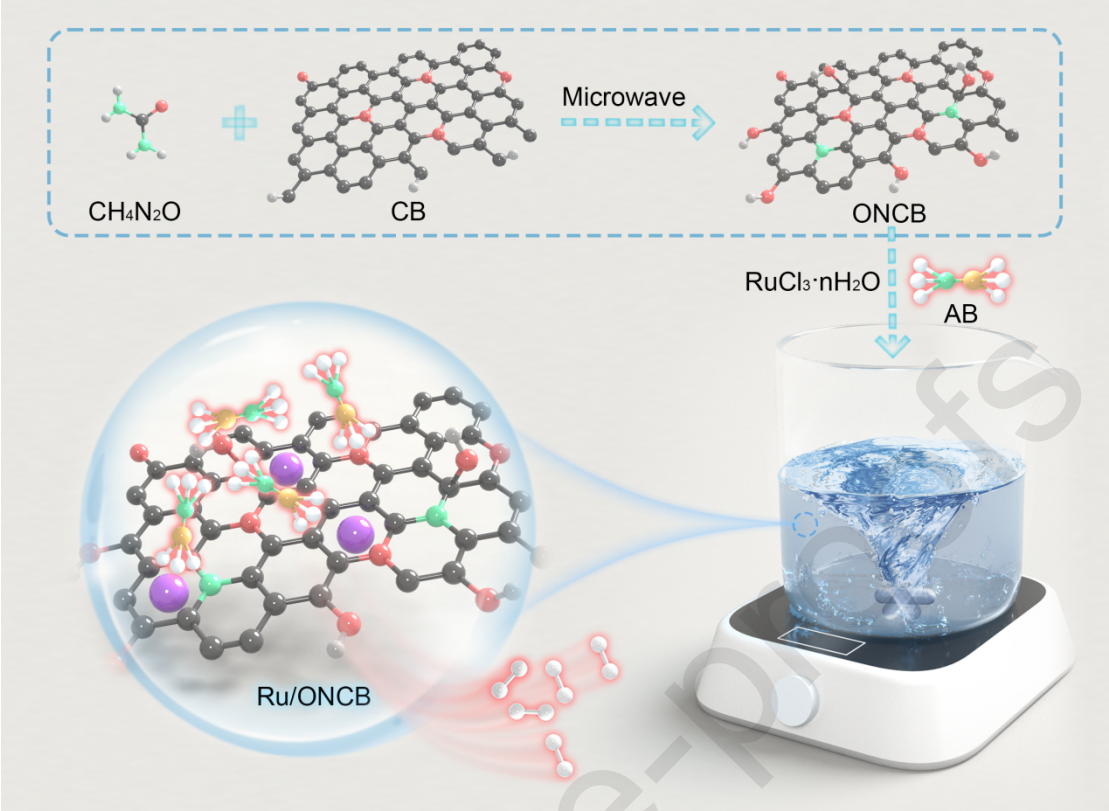

Fig. 1. Schematic diagram of synthetic program of Ru/ONCB for ABH.

exhibited similar spherical particle assemblies, indicating that the introduction of additional O and N dopants via microwave irradiation did not alter the properties of the pristine carbon matrix (Fig. 2a and 2d). The enlarged TEM image of Ru/ONCB revealed a uniform distribution of ultrafine Ru NPs with an average diameter of 2.2 ± 0.0 nm on the ONCB carrier (Fig. 2a-2c). In Ru/CB, the Ru NPs were also well distributed on CB; however, their particle size (3.1 ± 0.1 nm) was significantly larger (Fig. 2d-2f) compared to those in Ru/ONCB. The high-resolution TEM (HRTEM) image of Ru/ONCB displayed clear lattice fringes with a d-spacing of 0.22 nm (Fig. 2b inset), corresponding to the Ru (100) plane. Elemental mapping images of Ru/ONCB demonstrated an even distribution of N, O, and Ru throughout the ONCB carbon skeleton (Fig. 2g-2k). These results indicate that dual-doping of CB with O and N

promotes the formation of ultrasmall and uniformly distributed Ru NPs in Ru/ONCB, thereby enhancing the exposure of abundant surface-active sites for the reaction.

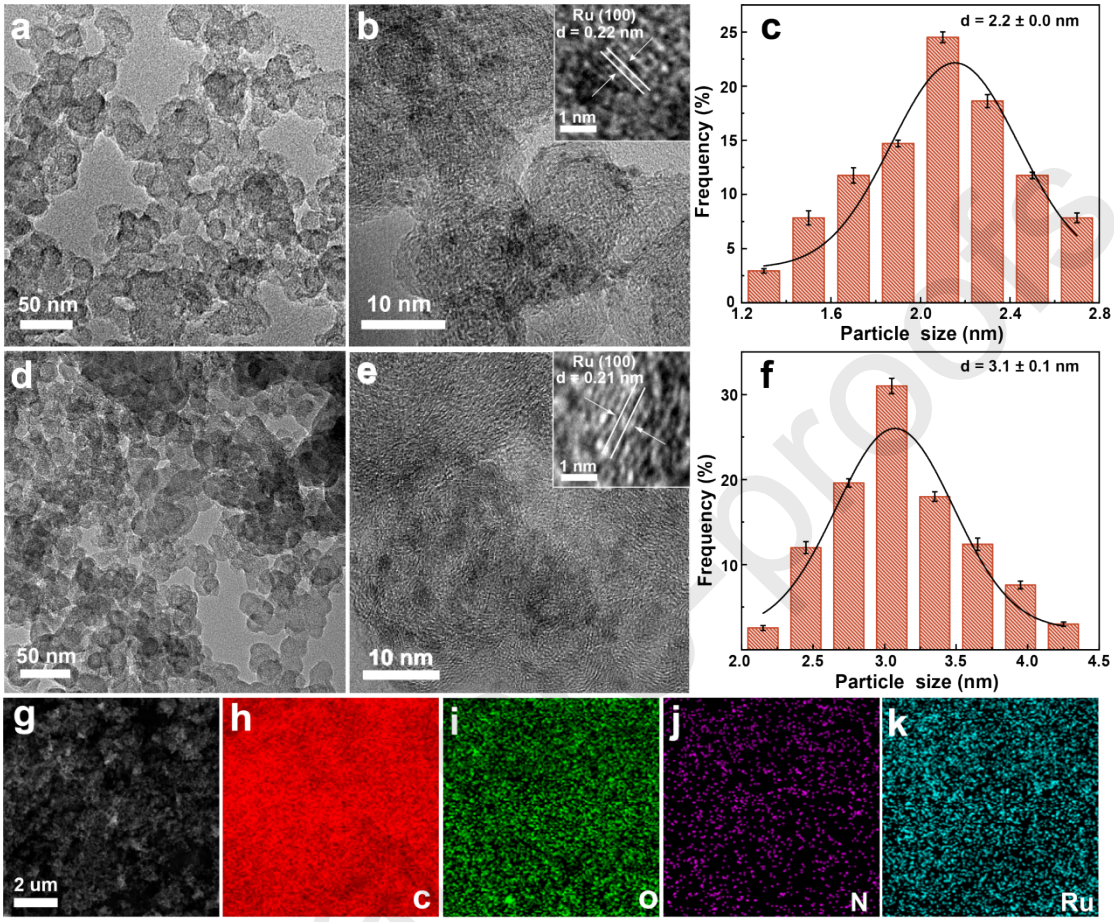

Fig. 2. TEM and HRTEM images of (a, b) Ru/ONCB and (d, e) Ru/CB. Size distribution of Ru for (c) Ru/ONCB and (f) Ru/CB. (g-k) Elemental mappings for Ru/ONCB. (Three repeated experiments were conducted under identical conditions)

The crystal structures of CB, ONCB, Ru/CB, and Ru/ONCB were characterized using X-ray diffraction (XRD). The XRD pattern of CB revealed two distinct diffraction peaks corresponding to the (002) and (010) planes of graphite carbon (Fig. 3a). Furthermore, the XRD patterns of ONCB and CB showed no significant differences, indicating that the introduction of N and O dopants did not alter the structure of CB. Additionally, the XRD pattern of Ru/ONCB did not exhibit any

obvious diffraction peaks of Ru species because of the low metal loading and/or high dispersion of Ru NPs. However, a weak characteristic peak of Ru was observed in the pattern of Ru/CB, suggesting the presence of relatively large Ru NPs, which is consistent with the TEM results. Fig. 3b presents the Raman spectra of Ru/ONCB and Ru/CB. The two diffraction peaks of Ru/ONCB at 1334.6 and 1583.4 cm^{-1} were ascribed to lattice defects (D band) of carbon and in-plane tensile vibration (G band) of sp^2 hybrid carbon, respectively. The I_D/I_G ratio of Ru/ONCB (1.3 ± 0.0) was significantly higher than that of Ru/CB (1.0 ± 0.0), reflecting an increase in defects due to microwave irradiation. Generally, a higher content of carbon defects can provide more anchoring sites for the active components, facilitating the formation of ultrafine and highly dispersed Ru NPs on the matrix [50]. The specific surface area, pore volume, and pore size distribution of Ru/ONCB and CB were investigated using N_2 adsorption/desorption measurements. The isothermal curves of Ru/ONCB exhibited typical type II isotherms with H_3 hysteresis loops, indicating the presence of abundant mesopores and macropores, as well as a few micropores (Fig. 3c). The likelihood of Ru NPs entering the pores of ONCB increases with the enlargement of the mesopores. This pore confinement effect enhances the full exposure of the active sites, leading to a high performance [51]. In comparison to CB, ONCB displayed several prominent peaks corresponding to the meso/macro pores (10-100 nm) on the pore distribution curve (Fig. 3d), suggesting that microwave irradiation plays a critical role in the formation of these unique pores. Previous literature indicates that increased porosity can enhance ion diffusion and mass transfer, thereby accelerating catalytic reactions [52]. Compared to

the original CB, ONCB exhibited slight increases in both pore volume and average pore size, likely benefiting from the introduction of nitrogen and the unfolding of the carbon structure [53]. However, the specific surface area decreased, which may be attributed to the occupation of carbon pores by Ru NPs [54] (Table S1). These findings suggest that urea functions not only as the nitrogen source but also as a pore-forming agent due to the generation of ammonia gas during Joule heating. Additionally, the specific surface area, pore volume, and pore diameter of Ru/ONCB were measured at 146.6 ± 5.2 m^2/g, 0.6 ± 0.0 cm^3/g, and 14.8 ± 0.5 nm, respectively. These results demonstrate that the synthesized Ru/ONCB possesses a large specific surface area and high porosity, which can provide more surface-exposed active sites and facilitate electron transfer, while also restricting the aggregation of Ru NPs. Consequently, this contributes to the effective transfer of reactants and products [55], ultimately enhancing catalytic performance.

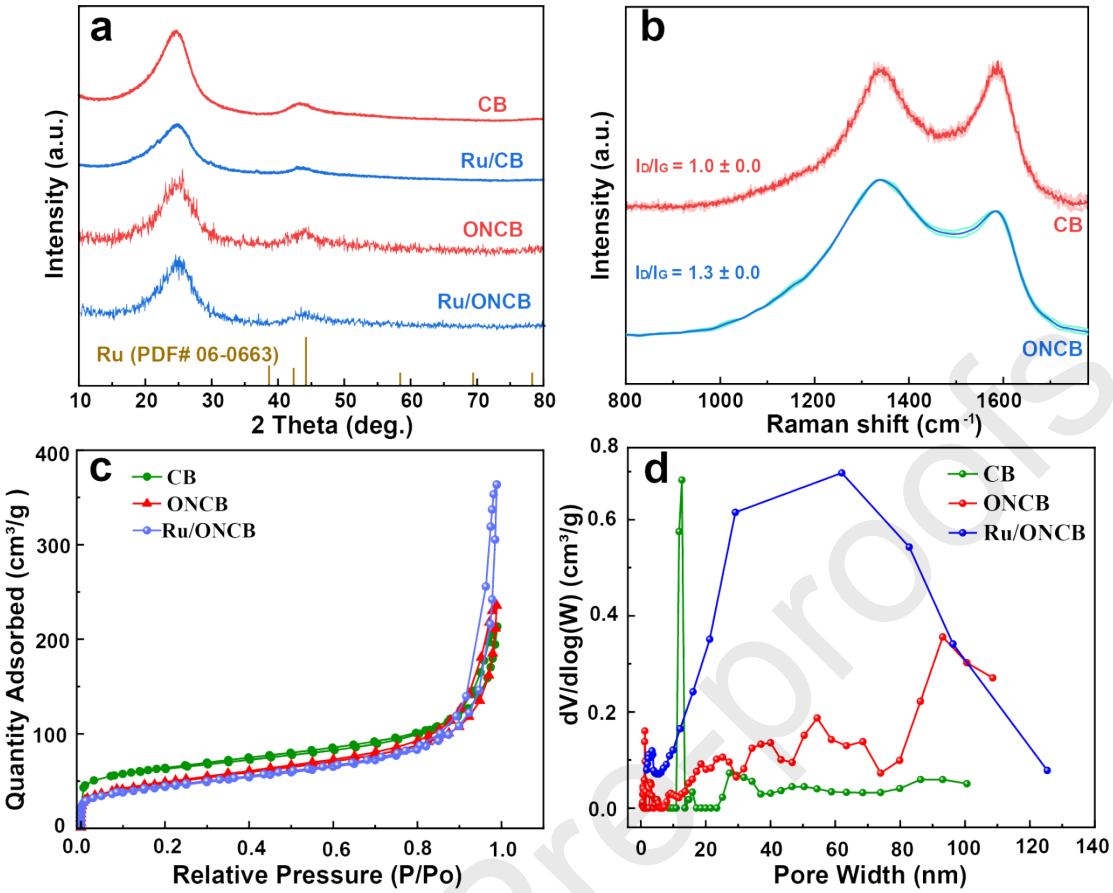

Fig. 3. (a) XRD patterns, (b) Raman spectra, (c) N_2 adsorption/desorption isotherm and (d) pore size distribution for the samples. (Three repeated experiments were conducted under identical conditions)

The elemental composition and surface chemical environment of Ru/ONCB and Ru/CB were analyzed using X-ray photoelectron spectroscopy (XPS). The presence of C, O, Ru and N in Ru/ONCB was clearly observed (Fig. 4a), confirming the successful incorporation of N and O onto the CB matrix. Furthermore, Ru/ONCB exhibited a nitrogen content of 2.1 ± 0.1 wt% and a higher oxygen content (6.3 ± 0.3 wt%) compared to Ru/CB (4.8 ± 0.4 wt%) (Table S2). This indicates that nitrogen was successfully incorporated into Ru/ONCB, and the carbon surface experienced an increase in oxygen-containing functional groups after microwave irradiation. The C 1s

spectra displayed four peaks (Fig. 4b), corresponding to C = C (284.7 eV), C-C (285.5 eV), C-O (286.5 eV), and -COO (289.6 eV) [56-58]. The contents of C-O and-COO groups on the surface of Ru/ONCB were 10.4% and 7.9%, respectively, while those on Ru/CB were 6.9% and 3.2%, respectively. Therefore, microwave irradiation facilitated the introduction of more oxygen-containing functional groups into ONCB. The O 1s spectra exhibited three peaks at 531.7 eV, 532.7 eV, and 534.1 eV (Fig. 4c), attributing to C = O, C-OH/C-O and O-C = O [56, 57, 59], respectively. Additionally, the O 1s binding energy of Ru/ONCB was negatively shifted by about 0.3 eV compared to Ru/CB, indicating a stronger electron interaction in Ru/ONCB [60]. The Ru 3p spectrum of Ru/CB (Fig. 4d) revealed four components: two peaks at 462.7 eV and 484.5 eV were assigned to Ru^0 $3p_{3/2}$ and Ru^0 $3p_{1/2}$, while the other two peaks at 466.7 eV and 488.7 eV were ascribed to Ru^{n+} $3p_{3/2}$ and Ru^{n+} $3p_{1/2}$ [61], respectively. Moreover, the binding energies of Ru^0 $3p_{3/2}$ and Ru^0 $3p_{1/2}$ in Ru/ONCB were relatively elevated, consistent with the observed shift in binding energies of O 1s. The N 1s spectrum of Ru/ONCB was deconvoluted into three peaks at 398.3 eV, 399.9 eV, and 401.0 eV corresponding to pyridine N, pyrrole N and graphite N, respectively (Fig. 4e) [62]. The contact angles of CB and ONCB were measured to investigate the changes in hydrophilicity after microwave irradiation. Compared with CB (124 ± 3 °), the contact angle of ONCB exhibited a slight decrease (101 ± 4 °), indicating that microwave irradiation treatment enhances the hydrophilicity of the carbon matrix (Fig. 4f). The introduction of abundant O and N functional groups not only facilitates the anchoring of Ru ions and prevents the aggregation of Ru NPs but also improves the hydrophilicity

of the catalyst, thereby alleviating mass transfer limitations [56].

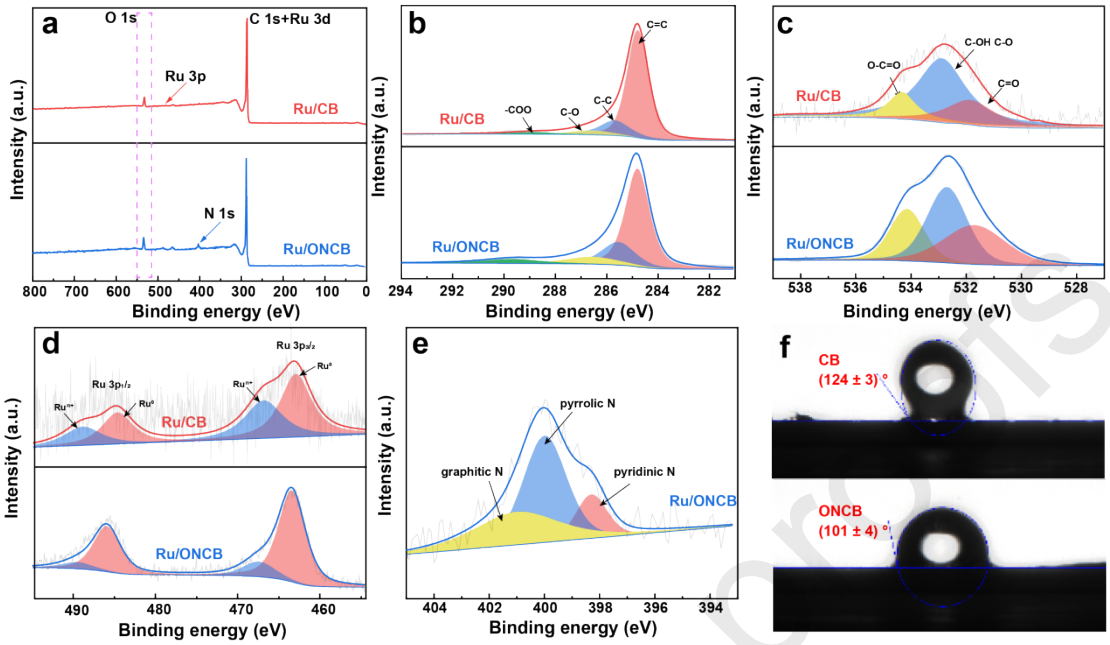

Fig. 4. (a) XPS survey spectra of Ru/CB and Ru/ONCB. High-resolution XPS spectra of (b) C 1s, (c) O 1s, (d) Ru 3p, and (e) N 1s for Ru/ONCB. (f) The contact angle of CB and ONCB. (Three repeated experiments were conducted under identical conditions)

The catalytic performance of the Ru/ONCB-20, Ru/ONCB-30, Ru/ONCB, and Ru/ONCB-50 catalysts, prepared using ONCB supports treated with varying microwave irradiation times, was investigated for hydrogen generation from ABH. Among these catalysts, Ru/ONCB demonstrated the highest catalytic activity, achieving a high TOF of 1763 ± 55 min^{-1} (Fig. 5a and 5b). This finding suggests that the duration of microwave treatment influences the surface microenvironment of carbon materials through the doping of O and N atoms, thereby regulating the catalytic activity of Ru NPs supported on heteroatom-modified carbon matrices. To identify the optimal metal loading in Ru/ONCB, control samples with different Ru loadings (0.4 wt%, 0.8 wt%, 1.2 wt%, and 1.6 wt%) were utilized as catalysts for hydrogen evolution

from ABH. As the Ru loading increased from 0.4 wt% to 1.2 wt%, the rate of H_2 production from ABH also increased, along with the corresponding TOF values (Fig. 5c and 5d). This enhancement can be ascribed to the increase in active sites available for the reaction. However, when the Ru loading reached 1.6 wt%, the catalyst exhibited a lower TOF value and only a slight improvement in the rate of ABH compared to the sample with a 1.2 wt% Ru loading. This decline may be due to the potential aggregation and size increase of Ru NPs [35]. Consequently, Ru/ONCB with a 1.2 wt% Ru loading was selected as the optimal catalyst for subsequent tests. To further elucidate the high activity of Ru/ONCB, a series of comparative experiments were conducted. The catalytic activity of CB, OCB, and ONCB materials for ABH was minimal, indicating that Ru was the active component (Fig. 5e). Upon the incorporation of Ru onto these materials, the Ru/ONCB catalyst exhibited superior catalytic activity (1763 ± 55 min^{-1}) compared with that of Ru/CB (548 ± 15 min^{-1}) and Ru/OCB (1067 ± 46 min^{-1}) (Fig. 5f). This observation indicates that the dual doping of O and N synergistically enhances the number of surface-exposed active sites and improves mass transfer during the reaction, thereby augmenting catalytic activity.

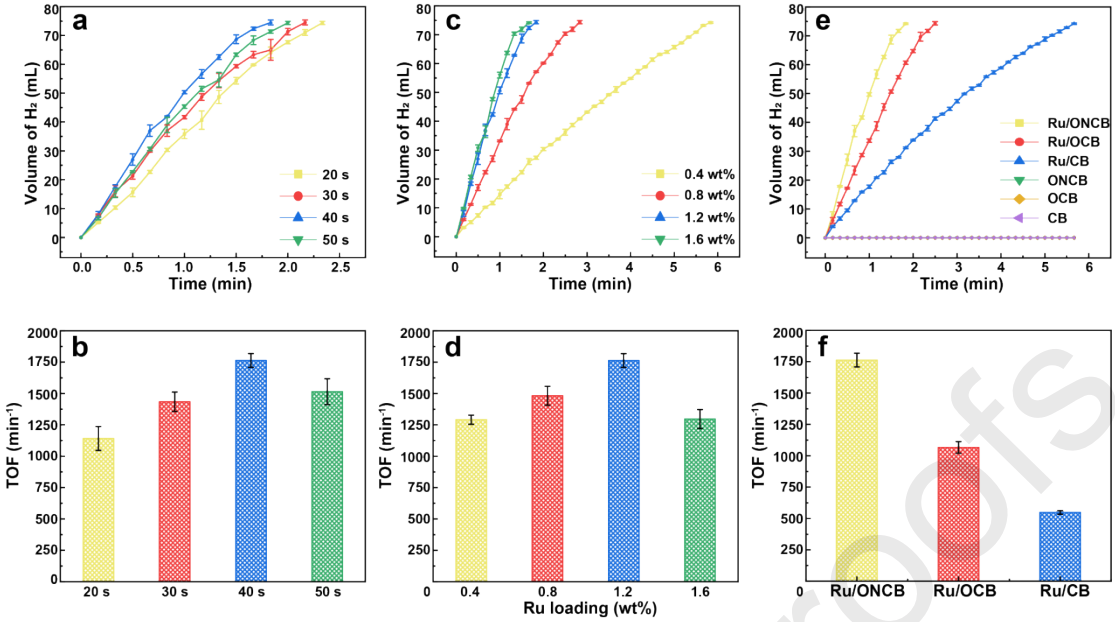

Fig. 5. (a) H_2 generation volume versus time over Ru/ONCB prepared at different microwave times for ABH, (b) the corresponding TOF values of (a). (c) H_2 generation volume versus time over Ru/ONCB prepared at different Ru loadings for ABH, (d) the corresponding TOF values of (c). (e) H_2 generation volume versus time over different catalysts for ABH, and (f) the corresponding TOF values of (e). (Three repeated experiments were conducted under identical conditions)

The hydrolysis kinetics of ABH were investigated under various concentrations of Ru, substrate contents, and reaction temperatures. It was initially observed that the rate of H_2 generation increased with higher Ru concentrations, indicating an increase in the number of surface-exposed active sites (Fig. 6a). The maximum TOF value of 1899 ± 36 min^{-1} was achieved at a Ru concentration of 0.9 mM. A linear relationship between the H_2 generation rate and Ru concentration was established (Fig. 6b), with a slope of 1.01, indicating that the ABH reaction follows first-order kinetics with respect to Ru concentration, consistent with previous reports [63]. The initial rate of H_2 release showed minimal variation with increasing AB concentration (Fig. 6c). Moreover, the

logarithmic plot of the H_2 release rate against initial AB concentration yielded a slope of 0.08 (Fig. 6d), demonstrating that ABH follows a zero-order reaction regarding AB concentration [62]. The H_2 release rate gradually increased as the reaction temperature was raised from 20 °C to 35 °C (Fig. 6e), which can be attributed to the enhanced collision probability of reactants and intermediates at elevated temperatures. Additionally, the E_a value calculated using the Arrhenius equation was determined to be 31.2 kJ/mol (Fig. 6f), which is lower than that of most reported Ru-based catalysts (Table S3), indicating a reduced energy barrier for hydrogen evolution from ABH. Furthermore, the Ru/ONCB catalyst exhibited the optimal TOF of 1899 ± 36 min^{-1}, significantly surpassing that of $Ru_{0.85}Pd_{0.15}/gC_3N_4$ (948 min^{-1}) [61], Ru@Co/C (320 min^{-1}) [64], Ru^0/ZrO_2 (173 min^{-1}) [35], and Ru/graphene (600 min^{-1}) [65]. Additional comparative results are presented in Table S3.

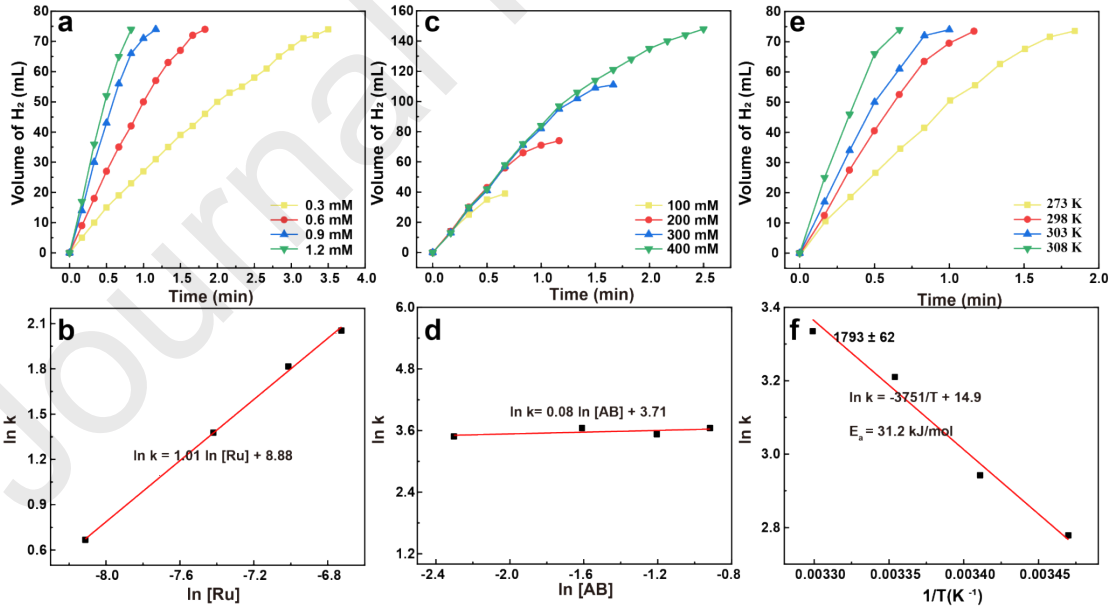

Fig. 6. H_2 generation volume versus time for ABH over Ru/ONCB under various (a) Ru concentrations, (c) AB contents, and (e) reaction temperatures. The logarithmic plots of (b)ln k versus ln [Ru] and (d) ln k versus ln [AB], and (f) the Arrhenius plot (ln

k versus 1/T).

To elucidate the mechanism of the ABH reaction, two aspects of the studies were implemented. Firstly, a kinetic isotope experiment was carried out using D_2O as the reaction solvent. The catalytic efficiency of the Ru/ONCB catalyst was significantly diminished when D_2O replaced H_2O (Fig. 7a). The corresponding TOF of 820 ± 13 min^{-1} was substantially lower than that in H_2O (1899 ± 36 min^{-1}) (Fig. 7b). Additionally, the calculated kinetic isotope effect (KIE) value of 2.13 ± 0.10 (Fig. 7b) further confirms that the RDS in the ABH reaction catalyzed by Ru/ONCB is the oxidative cleavage of O-H bonds in H_2O [66]. Secondly, the influence of OH^- on the catalytic performance of Ru/ONCB for ABH was investigated by varying the dosage of NaOH, with the optimal dosage reaching 0.60 g, resulting in a TOF of 5742 ± 81 min^{-1}, which is approximately three times higher than that observed without NaOH addition (Fig. 7d). However, the TOF value began to decline when the NaOH dosage was further increased. To ensure complete hydrogen production from ABH in an alkaline environment, the potential for ammonia production from ABH was examined using the indigo phenol blue method [67]. A more detailed description of the test method is provided in Text S1. Based on the UV-Vis absorption spectra and calibration curves of the standard concentration NH_4^+ solution (Fig. S1), only a trace amount of ammonia (1.3×10^{-5} mmol) was detected, indicating that AB was almost entirely converted to hydrogen. The effect of adding NaOH can be attributed to the interaction of an optimal quantity of OH^- ions with the surface of active Ru NPs, which creates an electron-rich environment and promotes the oxidation of H_2O [68]. However, an excessively high

concentration of NaOH can lead to over-coordination, wherein OH^- ions occupy too many active sites, resulting in a decrease in catalytic activity [69].

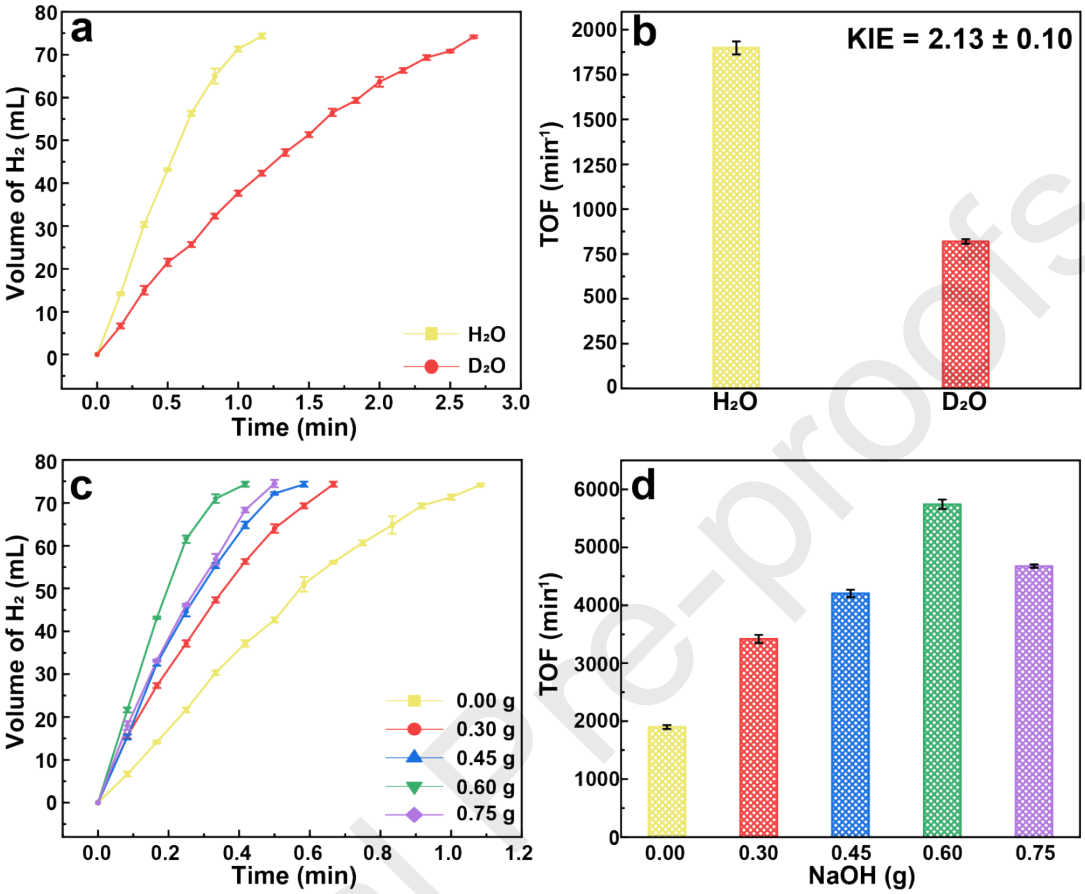

Fig. 7. (a) H_2 generation volume versus time for ABH over Ru/ONCB in H_2O and D_2O and (b) corresponding TOFs of (a). (c) H_2 generation volume versus time for ABH by Ru/ONCB under different NaOH dosages and (d) corresponding TOFs of (c). (Three repeated experiments were conducted under identical conditions)

The reusability of the ABH for hydrogen production over the Ru/ONCB catalyst was investigated through five consecutive cycles. During these reusability tests, a slight decline in the H_2 generation rate was observed (Fig. 8a). Notably, the Ru/ONCB catalyst retained 68 ± 1% of its initial catalytic activity after five cycles (Fig. 8b), indicating that the ONCB carrier effectively stabilizes the Ru NPs. To elucidate the

reasons behind the catalyst deactivation during successive reactions, several analyses were conducted. Firstly, the supernatant after the fifth cycle was analyzed using ICP-OES to assess the amount of Ru leaching. The results indicated negligible Ru leaching, suggesting that it has an insignificant impact on the decreased activity of Ru/ONCB during the recycling tests. Subsequently, the catalyst that underwent five cycles was collected and characterized. The structural stability of Ru in the Ru/ONCB catalyst during the reusability test was investigated using XRD. The recovered catalyst exhibited an identical XRD pattern compared to the fresh catalyst (Fig. S2), with no diffraction peaks corresponding to Ru species observed. This finding indicates the high structural stability of Ru within the Ru/ONCB catalyst. However, it was noted that Ru NPs displayed slight aggregation on ONCB, with a higher average diameter of 2.8 ± 0.0 nm (Fig. 8c and 8d) compared to fresh Ru/ONCB (2.2 ± 0.0 nm). This aggregation is believed to weaken the catalytic efficacy of Ru/ONCB. Furthermore, the degradation of catalytic activity may also be ascribed to an increasing number of metaborates covering the active sites, as well as potential catalyst loss during successive ABH reactions [70]. Considering the need for widespread application, enhancing the reusability of the Ru/ONCB catalyst is crucial.

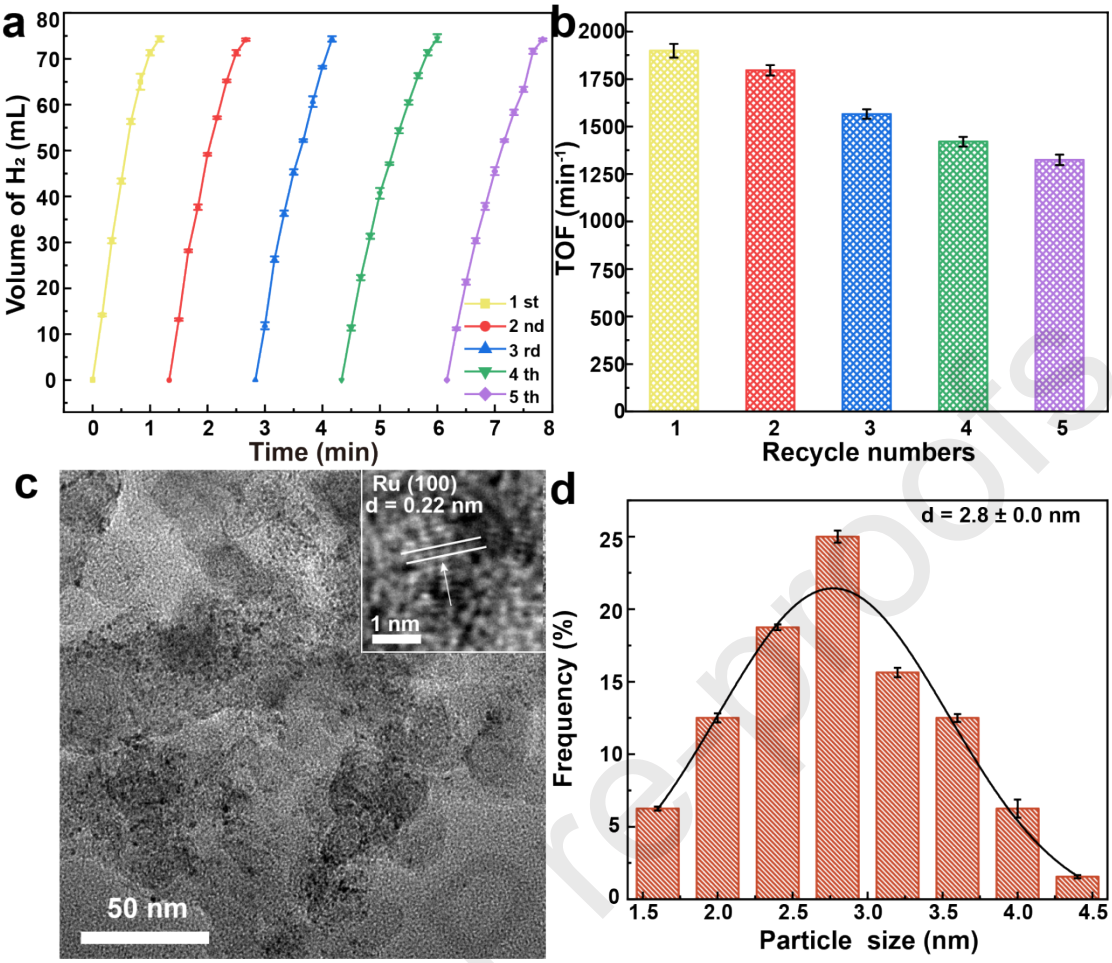

Fig. 8. (a) H_2 generation volume versus time for ABH upon Ru/ONCB from the first to fifth cycle. (b) corresponding TOFs of (a), (c) TEM and HRTEM images for Ru/ONCB after five cycles, and (d) corresponding size distribution of Ru for (c). (Three repeated experiments were conducted under identical conditions)

The reasons for the high activity of the Ru/ONCB catalyst are discussed based on the characterization results and performance tests. The active species, Ru NPs, are crucial in promoting ABH to produce hydrogen. Furthermore, the ONCB carrier effectively regulates the size and dispersion of Ru NPs. The incorporation of O and N heteroatomic groups enhances the hydrophilicity of the carbon support and increases the affinity of Ru^{3+} ions for the support, resulting in highly dispersed Ru NPs. Additionally, these

heteroatomic groups modulate the chemical and electronic properties of Ru NPs, leading to improved catalytic performance. The carbon material subjected to microwave radiation exhibits a larger specific surface area and higher porosity, which facilitates ion diffusion and mass transfer, generating more active sites, and thereby accelerating the rate of ABH. This study highlights the benefits of the solid-phase microwaving process. Utilizing a simple domestic microwave oven as the reactor provides an inexpensive, energy-efficient, and time-saving alternative compared to conventional synthetic methods [71]. The selected carbon materials can effectively couple with microwave radiation, enabling rapid temperature elevation and facilitating dual-doping with O and N in the microwave field [72-74]. The solid-phase microwaving process achieves results within seconds, whereas liquid-state synthetic processes typically require hours of microwave radiation [75, 76]. This solid-phase microwave heating approach, grounded in scientific principles, can be adapted to various microwave absorber precursors to enhance the surface microenvironment regulation and catalytic performance of supported metal nanomaterials.

4. Conclusions

In summary, a rapid and convenient methodology for synthesizing O and N co-doped CB support using microwave-assisted solid-state reaction with urea as the nitrogen source has been reported. Compared to conventional methods, the developed dual doping process is characterized by several key aspects: (a) the entire microwave irradiation is completed in an exceptionally short time of only 40 s, significantly reducing the catalysts preparation time; (b) the amount of urea utilized has been notably

minimized, and the absence of O-functional reagents not only enhances material utilization efficiency but also simplifies the process; and (c) no specialized equipment is required beyond a standard household microwave oven. Given these advantages, this method offers substantial benefits in catalyst preparation, including time and cost savings, as well as reduced operational complexity. The resulting ONCB support, characterized by its porous structure and abundant O/N dopants, plays an essential role in facilitating the growth of non-agglomerated Ru NPs. The optimized Ru/ONCB catalyst demonstrates an impressive TOF of 1899 ± 36 min^{-1} (4529 ± 238 min^{-1} based on Ru dispersion) in aqueous solution for ABH without the need for any alkali additives, surpassing many reported Ru-based catalysts [11, 35, 61, 65, 77, 78]. Experimental evidence confirms that RDS is the oxidative cleavage of O-H bonds in water rather than the destruction of B-N or B-H bonds in AB. The electronic interaction between uniformly dispersed Ru NPs and the well-designed ONCB support facilitates the oxidative cleavage of O-H bonds in water molecules, thereby enhancing the catalytic performance for ABH. Furthermore, the Ru/ONCB catalyst exhibits relatively good reusability for ABH. This study not only introduces an ultrafast and cost-effective solid-state microwave radiation strategy for the fabrication of efficient carbon-supported Ru NPs, but also provides a promising approach for effective hydrogen production. Future research could explore the feasibility of doping with other heteroatoms through microwave-assisted solid-state reactions, as well as the potential for employing alternative microwave absorbers.

References

[1] X.Y. Liu, J.W. Liu, G. Li, J.X. Zhao, Transition metal clusters with precise numbers of atoms anchored on graphdiyne as multifunctional electrocatalysts for OER/ORR/HER: a computational study, Rare Metals 43(7) (2024) 3107-3117.

[2] M.X. Li, J.T. Hu, H.B. Lu, A stable and efficient 3D cobalt-graphene composite catalyst for the hydrolysis of ammonia borane, Catalysis Science & Technology 6(19) (2016) 7186-7192.

[3] J.H. Shi, F. Qiu, W.B. Yuan, M.M. Guo, Z.H. Lu, Nitrogen-doped carbon-decorated yolk-shell CoP@FeCoP micro-polyhedra derived from MOF for efficient overall water splitting, Chemical Engineering Journal 403 (2021) 126312.

[4] Y.X. Luo, Q.F. Yang, W.D. Nie, Q.L. Yao, Z.J. Zhang, Z.H. Lu, Anchoring IrPdAu Nanoparticles on NH_2-SBA-15 for Fast Hydrogen Production from Formic Acid at Room Temperature, ACS Applied Materials & Interfaces 12(7) (2020) 8082-8090.

[5] Z.J. Zhang, Y.X. Luo, S.W. Liu, Q.L. Yao, S.J. Qing, Z.H. Lu, A PdAg-CeO_2 nanocomposite anchored on mesoporous carbon: a highly efficient catalyst for hydrogen production from formic acid at room temperature, Journal of Materials Chemistry A 7(37) (2019) 21438-21446.

[6] Y.F. Feng, Y.Z. Li, Q.Y. Liao, W.M. Zhang, Z.Q. Huang, X. Chen, Y.X. Shao, H.F. Dong, Q.B. Liu, H. Li, Modulation the electronic structure of hollow structured CuO-$NiCo_2O_4$ nanosphere for enhanced catalytic activity towards methanolysis of ammonia borane, Fuel 332 (2023) 126045.

[7] J.Y. Liao, Y.X. Shao, Y.F. Feng, J. Zhang, C.X. Song, W. Zeng, J.T. Tang, H.F. Dong, Q.B. Liu, H. Li, Interfacial charge transfer induced dual-active-sites of

heterostructured $Cu_{0.8}Ni_{0.2}WO_4$ nanoparticles in ammonia borane methanolysis for fast hydrogen production, Applied Catalysis B-Environmental 320 (2023) 121973.

[8] W.L. Yu, N.J. Fang, R.B. Wang, Z.B. Liu, Y.H. Chu, C.X. Huang, Molecule dipole and steric hindrance engineering to modulate electronic structure of PTCDA/PTA for highly efficient photocatalytic hydrogen evolution and antibiotics degradation, Advanced Functional Materials 34(17) (2024) 2314894.

[9] J. Deng, X.L. Zhou, J.D. Zou, Y.Q. Qin, P.C. Wang, PdCo alloy supported on a ZIF-derived N-doped carbon hollow polyhedron for dehydrogenation of ammonia borane, ACS Applied Energy Materials 5(6) (2022) 7408-7419.

[10] Q.L. Yao, Z.H. Lu, Y.W. Yang, Y.Z. Chen, X.S. Chen, H.L. Jiang, Facile synthesis of graphene-supported Ni-CeO_x nano-composites as highly efficient catalysts for hydrolytic dehydrogenation of ammonia borane, Nano Research 11(8) (2018) 4412-4422.

[11] E.B. Kalkan, S. Akbayrak, S. Özkar, Ruthenium(0) nanoparticles supported on nanohafnia: A highly active and long-lived catalyst in hydrolytic dehydrogenation of ammonia borane, Molecular Catalysis 430 (2017) 29-35.

[12] S. Akbayrak, S. Özkar, Ammonia borane as hydrogen storage materials, International Journal of Hydrogen Energy 43(40) (2018) 18592-18606.

[13] S. Akbayrak, Y. Tonbul, S. Özkar, Ceria supported rhodium nanoparticles: Superb catalytic activity in hydrogen generation from the hydrolysis of ammonia borane, Applied Catalysis B: Environmental 198 (2016) 162-170.

[14] H. Lv, R. Wei, X.W. Guo, L.Z. Sun, B. Liu, Synergistic catalysis of binary RuP

nanoclusters on nitrogen-functionalized hollow mesoporous carbon in hydrogen production from the hydrolysis of ammonia borane, Journal of Physical Chemistry Letters 12(1) (2021) 696-703.

[15] M. Navlani-García, D. Salinas-Torres, D. Cazorla-Amorós, Hydrolytic dehydrogenation of ammonia borane attained by Ru-based catalysts: An auspicious option to produce hydrogen from a solid hydrogen carrier molecule, Energies 14(8) (2021) 2199.

[16] N. Tunç, M. Rakap, Preparation and characterization of Ni-M (M: Ru, Rh, Pd) nanoclusters as efficient catalysts for hydrogen evolution from ammonia borane methanolysis, Renewable Energy 155 (2020) 1222-1230.

[17] Y.M. Peng, Y.T. He, Y. Wang, Y. Long, G.Y. Fan, Sustainable one-pot construction of oxygen-rich nitrogen-doped carbon nanosheets stabilized ultrafine Rh nanoparticles for efficient ammonia borane hydrolysis, Journal of Colloid and Interface Science 594 (2021) 131-140.

[18] W.Y. Chen, J. Ji, X. Feng, X.Z. Duan, G. Qian, P. Li, X.G. Zhou, D. Chen, W.K. Yuan, Mechanistic insight into size-dependent activity and durability in Pt/CNT catalyzed hydrolytic dehydrogenation of ammonia borane, Journal of the American Chemical Society 136(48) (2014) 16736-16739.

[19] R. Wei, Z.C. Chen, H. Lv, X.C. Zheng, X. Ge, L.Z. Sun, K. Song, C.C. Kong, W. Zhang, B. Liu, Ultrafine RhNi nanocatalysts confined in hollow mesoporous carbons for a highly efficient hydrogen production from ammonia borane, Inorganic Chemistry 60(9) (2021) 6820-6828.

[20] X.W. Guo, X. Chen, Y.P. Huang, X.W. Min, C.C. Kong, Y.W. Tang, B. Liu, Atomically ordered Rh_2P catalysts anchored within hollow mesoporous carbon for efficient hydrogen production, Chemical Communications 57(92) (2021) 12345-12348.

[21] R. Ding, Q. Chen, Q. Luo, L.X. Zhou, Y. Wang, Y. Zhang, G.Y. Fan, Salt template-assisted in situ construction of Ru nanoclusters and porous carbon: excellent catalysts toward hydrogen evolution, ammonia-borane hydrolysis, and 4-nitrophenol reduction, Green Chemistry 22(3) (2020) 835-842.

[22] S. Özkar, Increasing the catalytic efficiency of rhodium(0) nanoparticles in hydrolytic dehydrogenation of ammonia borane, International Journal of Hydrogen Energy 54 (2024) 327-343.

[23] S. Akbayrak, S. Oezkar, Palladium nanoparticles supported on cobalt(II,III) oxide nanocatalyst: High reusability and outstanding catalytic activity in hydrolytic dehydrogenation of ammonia borane, Journal of Colloid and Interface Science 626 (2022) 752-758.

[24] W.F. Chen, G. Lv, J.R. Fu, H.Y. Ren, J.L. Shen, J. Cao, X. Liu, Demonstration of controlled hydrogen release using Rh@GQDs during hydrolysis of NH_3BH_3, ACS Applied Materials & Interfaces 13(42) (2021) 50017-50026.

[25] Y. Tonbul, S. Akbayrak, S. Özkar, Magnetically separable rhodium nanoparticles as catalysts for releasing hydrogen from the hydrolysis of ammonia borane, Journal of Colloid and Interface Science 553 (2019) 581-587.

[26] S. Akbayrak, S. Özkar, Cobalt ferrite supported platinum nanoparticles: Superb catalytic activity and outstanding reusability in hydrogen generation from the

hydrolysis of ammonia borane, Journal of Colloid and Interface Science 596 (2021) 100-107.

[27] S. Özkar, A review on platinum(0) nanocatalysts for hydrogen generation from the hydrolysis of ammonia borane, Dalton Transactions 50(36) (2021) 12349-12364.

[28] S. Akbayrak, S. Özkar, Magnetically isolable Pt^0/Co_3O_4 nanocatalysts: outstanding catalytic activity and high reusability in hydrolytic dehydrogenation of ammonia borane, ACS Applied Materials & Interfaces 13(29) (2021) 34341-34348.

[29] S. Akbayrak, Y. Tonbul, S. Özkar, Magnetically separable Rh^0/Co_3O_4 nanocatalyst provides over a million turnovers in hydrogen release from ammonia borane, ACS Sustainable Chemistry & Engineering 8(10) (2020) 4216-4224.

[30] A.H.Y. Al-Areedhee, S. Karaboga, I.A. Morkan, S. Özkar, Nanotitania supported ruthenium(0) nanoparticles as active catalyst for releasing hydrogen from dimethylamine borane, International Journal of Hydrogen Energy 51 (2024) 1097-1108.

[31] J. Jiang, W. Wei, Z. Ren, Y. Luo, X.Z. Wang, Y. Xu, M.M. Chang, L.H. Ai, Facile construction of robust Ru-Co_3O_4 Mott-Schottky catalyst enabling efficient dehydrogenation of ammonia borane for hydrogen generation, Journal of Colloid and Interface Science 646 (2023) 25-33.

[32] W.D. Li, Y.X. Zhao, Y. Liu, M.Z. Sun, G.I.N. Waterhouse, B.L. Huang, K. Zhang, T.R. Zhang, S.Y. Lu, Exploiting Ru-induced lattice strain in CoRu nanoalloys for robust bifunctional hydrogen production, Angewandte Chemie-International Edition 60(6) (2021) 3290-3298.

[33] L.C. Liang, L.Y. Bian, Y.P. Fan, S.Y. Guan, X.Y. Liu, Q.Y. Sun, B.Z. Liu,

Nitrogen doping excited Ru and $Ti_3C_{2-x}N_x$ support for hydrogen generation from ammonia borane, Fuel 339 (2023) 127445.

[34] Y.L. Meng, Q.H. Sun, T.J. Zhang, J.C. Zhang, Z.Y. Dong, Y.H. Ma, Z.X. Wu, H.F. Wang, X.G. Bao, Q.M. Sun, J.H. Yu, Cobalt-promoted noble-metal catalysts for efficient hydrogen generation from ammonia borane hydrolysis, Journal of the American Chemical Society 145 (2023) 5486-5495.

[35] Y. Tonbul, S. Akbayrak, S. Özkar, Nanozirconia supported ruthenium(0) nanoparticles: Highly active and reusable catalyst in hydrolytic dehydrogenation of ammonia borane, Journal of Colloid and Interface Science 513 (2018) 287-294.

[36] H. Wen, R.F. Shen, Y.Y. Liu, X.Y. Huang, S.L. Liu, Z.K. Peng, X.L. Wu, X.J. Guo, E. Liang, H.Y. Yuan, B.J. Li, J.C. Jiang, Insights into boosting catalytic hydrogen evolution over Co doping Ru nanoparticles, Fuel 351 (2023) 128950.

[37] S.L. Yang, Y. Zhu, J.X. Liu, X.C. Zheng, X.L. Zhang, P. Liu, Highly efficient catalytic hydrolysis of NH_3BH_3 over Ru nanoparticles anchored to chitosan-h-BN composite, International Journal of Hydrogen Energy 48(49) (2023) 18708-18718.

[38] C.L. Xu, M. Ming, Q. Wang, C. Yang, G.Y. Fan, Y. Wang, D.J. Gao, J. Bi, Y. Zhang, Facile synthesis of effective Ru nanoparticles on carbon by adsorption-low temperature pyrolysis strategy for hydrogen evolution, Journal of Materials Chemistry A 6(29) (2018) 14380-14386.

[39] M. Rakap, PVP-stabilized Ru-Rh nanoparticles as highly efficient catalysts for hydrogen generation from hydrolysis of ammonia borane, Journal of Alloys and Compounds 649 (2015) 1025-1030.

[40] H. Can, Ö. Metin, A facile synthesis of nearly monodisperse ruthenium nanoparticles and their catalysis in the hydrolytic dehydrogenation of ammonia borane for chemical hydrogen storage, Applied Catalysis B-Environmental 125 (2012) 304-310.

[41] C. Ruiz-Garcia, F. Heras, L. Calvo, N. Alonso-Morales, J.J. Rodriguez, M.A. Gilarranz, Improving the activity in hydrodechlorination of Pd/C catalysts by nitrogen doping of activated carbon supports, Journal of Environmental Chemical Engineering 8(2) (2020) 103689.

[42] S. Akbayrak, Z. Özçifçi, A. Tabak, Noble metal nanoparticles supported on activated carbon: Highly recyclable catalysts in hydrogen generation from the hydrolysis of ammonia borane, Journal of Colloid and Interface Science 546 (2019) 324-332.

[43] M. Xiao, M.T. Pang, Y. Peng, B.C. Hao, Y. Liao, H. Mao, F.W. Huo, Zeolitic imidazolate framework-8 templated synthesis of a heterogeneous Pd catalyst for remediation of chlorophenols pollution, Chemical Communications 56(21) (2020) 3143-3146.

[44] M. Mazurkiewicz-Pawlicka, A. Malolepszy, A. Mikolajczuk-Zychora, B. Mierzwa, A. Borodzinski, L. Stobinski, A simple method for enhancing the catalytic activity of Pd deposited on carbon nanotubes used in direct formic acid fuel cells, Applied Surface Science 476 (2019) 806-814.

[45] C.G. Hu, L.M. Dai, Doping of carbon materials for metal-free electrocatalysis, Advanced Materials 31(7) (2019) 1804672.

[46] X.L. Zhang, Z.W. Ni, X.X. Bai, H.T. Shen, Z.R. Wang, C.L. Wei, K.D. Tian, B.J. Xi, S.L. Xiong, J.K. Feng, Hierarchical porous N-doped carbon encapsulated fluorine-free MXene with tunable coordination chemistry by one-pot etching strategy for lithium-sulfur batteries, Advanced Energy Materials 13(29) (2023) 2301349.

[47] S. Nagasawa, M. Yudasaka, K. Hirahara, T. Ichihashi, S. Iijima, Effect of oxidation on single-wall carbon nanotubes, Chemical Physics Letters 328(4) (2000) 374-380.

[48] W. Li, K.L. Wang, S.J. Cheng, K. Jiang, Self-polymerized disordered carbon enabling high sodium storage performance through expanded interlayer spacing by bound sulfur atoms, Chemelectrochem 5(21) (2018) 3206-3212.

[49] X. Li, Y.C. Yan, Y. Jiang, X.Q. Wu, S. Li, J.B. Huang, J.J. Li, Y.F. Lin, D.R. Yang, H. Zhang, Ultra-small Rh nanoparticles supported on WO_{3-x} nanowires as efficient catalysts for visible-light-enhanced hydrogen evolution from ammonia borane, Nanoscale Advances 1(10) (2019) 3941-3947.

[50] C.X. Li, Z.B. Liu, N.J. Fang, W.L. Yu, C.F. Yang, Y.H. Chu, W. Liu, Extrinsic defects-rich biochar for efficient peroxydisulfate activation: Electronic structure modulation and disparate nonradical mechanisms, Separation and Purification Technology 336 (2024) 126338.

[51] X.F. Ma, H. Xiao, Y.Y. Jing, Y. Gao, Y.L. He, M. Zhao, J.F. Jia, H.S. Wu, Site difference influence of anchored Ru in mesoporous carbon on electrocatalytic performance toward pH-universal hydrogen evolution reaction, Rare Metals 42(12) (2023) 4015-4028.

[52] H. Lv, L. Sun, D. Xu, W. Li, B. Huang, B. Liu, Precise synthesis of hollow

mesoporous palladium–sulfur alloy nanoparticles for selective catalytic hydrogenation, CCS Chemistry 4(8) (2021) 2854-2863.

[53] H.Q. Zhou, X.W. Zhang, X.C. Zhang, F. Yuan, X.L. Wang, S.L. Yan, J.B. Wang, C.Q. Li, Z.M. Sun, N-doped microcrystalline graphite for boosting peroxymonosulfate activation with highly efficient degradation of bisphenol A, Carbon 216 (2024) 118579.

[54] Y.W. Wei, G. Yang, X.X. Xu, Y.Y. Liu, N.X. Kang, B.J. Li, Y.Z. Wang, Y.X. Zhao, Ultrafine Ru nanoparticles anchored on core-shell structured zeolite-carbon for efficient catalysis of hydrogen generation, Rare Metals 42(7) (2023) 2324-2334.

[55] F.Y. Zhong, Q. Wane, G.L. Xu, Y.C. Yang, Y. Wang, Y. Zhang, D.J. Gao, J. Bi, G.Y. Fan, Ultrafine and highly dispersed Ru nanoparticles supported on nitrogen-doped carbon nanosheets: Efficient catalysts for ammonia borane hydrolysis, Applied Surface Science 455 (2018) 326-332.

[56] M.Y. Mao, Q. Chen, J. Wu, G.Y. Fan, Anchoring and space-confinement effects to synthesize ultrasmall Pd nanoparticles for efficient ammonia borane hydrolysis, International Journal of Hydrogen Energy 45(51) (2020) 27244-27253.

[57] G. Zhong, S.M. Xu, Q. Dong, X.Z. Wang, L.B. Hu, Rapid, universal surface engineering of carbon materials via microwave-induced carbothermal shock, Advanced Functional Materials 31(18) (2021) 2010968.

[58] Q. Luo, Q. Chen, Y. Wang, Y. Long, W.D. Jiang, G.Y. Fan, Facile, general and environmental-friendly fabrication of O/N-codoped porous carbon as a universal matrix for efficient hydrogen evolution electrocatalysts, Chemical Engineering Journal 420 (2021) 130483.

[59] R. Ding, T.T. Yan, Y. Wang, Y. Long, G.Y. Fan, Carbon nanopore and anchoring site-assisted general construction of encapsulated metal (Rh, Ru, Ir) nanoclusters for highly efficient hydrogen evolution in pH-universal electrolytes and natural seawater, Green Chemistry 23(12) (2021) 4551-4559.

[60] F.K. Bi, X.D. Zhang, S. Xiang, Y.Y. Wang, Effect of Pd loading on ZrO_2 support resulting from pyrolysis of UiO-66: Application to CO oxidation, Journal of Colloid and Interface Science 573 (2020) 11-20.

[61] S.N. Yue, X.G. Wang, S.T. Li, Y. Sheng, X.J. Zou, X.G. Lu, C.L. Zhang, Highly selective hydrogenation of halogenated nitroarenes over Ru/CN nanocomposites by in situ pyrolysis, New Journal of Chemistry 44(27) (2020) 11861-11869.

[62] A. Guo, L. Hu, Y.M. Peng, Y. Wang, Y. Long, J.S. Fu, G.Y. Fan, Steam pretreatment-mediated catalytic activity modulation for ammonia borane hydrolysis over ruthenium nanoclusters on nitrogen/oxygen-rich carbon nanotubes, Applied Surface Science 579 (2022) 152158.

[63] J.T. Du, H. Niu, H. Wu, X.F. Zeng, J.X. Wang, J.F. Chen, PVP-stabilized platinum nanoparticles supported on modified silica spheres as efficient catalysts for hydrogen generation from hydrolysis of ammonia borane, International Journal of Hydrogen Energy 46(49) (2021) 25081-25091.

[64] N. Cao, J. Su, X.L. Hong, W. Luo, G.Z. Cheng, In situ facile synthesis of Ru-based core-shell nanoparticles supported on carbon black and their high catalytic activity in the dehydrogenation of amine-boranes, Chemistry-an Asian Journal 9(2) (2014) 562-571.

[65] C. Du, Q. Ao, N. Cao, L. Yang, W. Luo, G.Z. Cheng, Facile synthesis of monodisperse ruthenium nanoparticles supported on graphene for hydrogen generation from hydrolysis of ammonia borane, International Journal of Hydrogen Energy 40(18) (2015) 6180-6187.

[66] W.Y. Chen, D.L. Li, Z.J. Wang, G. Qian, Z.J. Sui, X.Z. Duan, X.G. Zhou, I. Yeboah, D. Chen, Reaction mechanism and kinetics for hydrolytic dehydrogenation of ammonia borane on a Pt/CNT catalyst, AICHE Journal 63(1) (2017) 60-65.

[67] C. He, Z.Y. Wu, L. Zhao, M. Ming, Y. Zhang, Y.P. Yi, J.S. Hu, Identification of FeN_4 as an efficient active site for electrochemical N_2 reduction, ACS Catalysis 9(8) (2019) 7311-7317.

[68] Q.L. Yao, K. Yang, X.L. Hong, X.S. Chen, Z.H. Lu, Base-promoted hydrolytic dehydrogenation of ammonia borane catalyzed by noble-metal-free nanoparticles, Catalysis Science & Technology 8(3) (2018) 870-877.

[69] X.F. Su, S.F. Li, PVP-stabilized Co-Ni nanoparticles as magnetically recyclable catalysts for hydrogen production from methanolysis of ammonia borane, International Journal of Hydrogen Energy 46(27) (2021) 14384-14394.

[70] Y.L. Ma, X.J. Li, Y. Zhang, L. Chen, J.T. Wu, D.J. Gao, J. Bi, G.Y. Fan, Ruthenium nanoparticles supported on TiO_2(B) nanotubes: Effective catalysts in hydrogen evolution from the hydrolysis of ammonia borane, Journal of Alloys and Compounds 708 (2017) 270-277.

[71] G. Zhong, S.M. Xu, M.J. Cui, Q. Dong, X.Z. Wang, Q.Q. Xia, J.L. Gao, Y. Pei, Y. Qiao, G. Pastel, T. Sunaoshi, B. Yang, L.B. Hu, Rapid, high-Temperature, in situ

microwave synthesis of bulk nanocatalysts, Small 15(47) (2019) 1904881.

[72] D. Voiry, J. Yang, J. Kupferberg, R. Fullon, C. Lee, H.Y. Jeong, H.S. Shin, M. Chhowalla, High-quality graphene via microwave reduction of solution-exfoliated graphene oxide, Science 353(6306) (2016) 1413-1416.

[73] G. Zhong, S.M. Xu, C.J. Chen, D.J. Kline, M. Giroux, Y. Pei, M.L. Jiao, D.P. Liu, R.Y. Mi, H. Xie, B. Yang, C. Wang, M.R. Zachariah, L.B. Hu, Synthesis of metal oxide nanoparticles by rapid, high-temperature 3D microwave heating, Advanced Functional Materials 29(48) (2019) 1904282.

[74] A.M. Schwenke, S. Hoeppener, U.S. Schubert, Synthesis and modification of carbon nanomaterials utilizing microwave heating, Advanced Materials 27(28) (2015) 4113-4141.

[75] L. Lu, X.F. Sun, J. Ma, D.X. Yang, H.H. Wu, B.X. Zhang, J.L. Zhang, B.X. Han, Highly efficient electroreduction of CO_2 to methanol on palladium-copper bimetallic aerogels, Angewandte Chemie-International Edition 57(43) (2018) 14149-14153.

[76] H. Zhao, Y.Y. Yuan, D. Zhang, Y.N. Qin, Y. Han, H.D. Li, Z.C. Wang, S.X. Li, J.P. Lai, L. Wang, Ultrafast generation of nanostructured noble metal aerogels by a microwave method for electrocatalytic hydrogen evolution and ethanol oxidation, ACS Applied Nano Materials 4(10) (2021) 11221-11230.

[77] R. Lu, C.L. Xu, Q. Wang, Y. Wang, Y. Zhang, D.J. Gao, J. Bi, G.Y. Fan, Ruthenium nanoclusters distributed on phosphorus-doped carbon derived from hypercrosslinked polymer networks for highly efficient hydrolysis of ammonia-borane, International Journal of Hydrogen Energy 43(39) (2018) 18253-18260.

[78] G.Y. Fan, Q.Q. Liu, D.M. Tang, X.J. Li, J. Bi, D.J. Gao, Nanodiamond supported Ru nanoparticles as an effective catalyst for hydrogen evolution from hydrolysis of ammonia borane, International Journal of Hydrogen Energy 41(3) (2016) 1542-1549.

Graphic Abstract

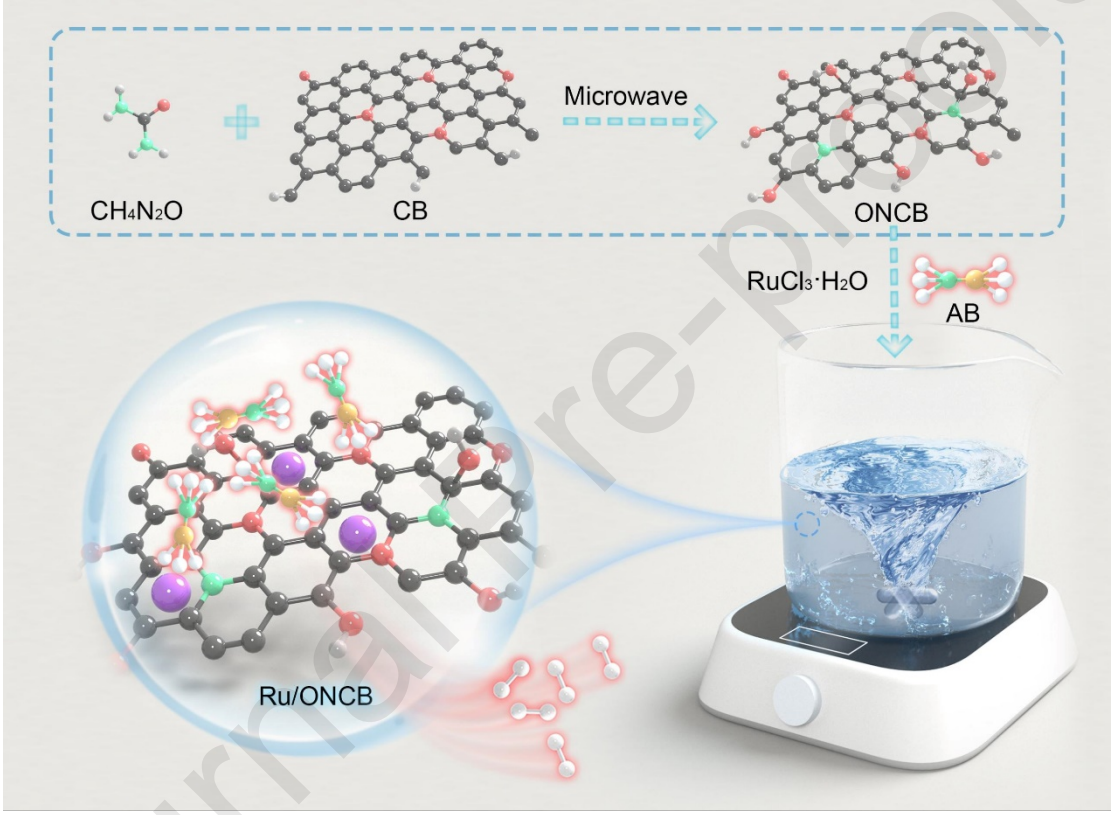

Declaration of interests

☒ The authors declare that they have no known competing financial interests or personal relationships that could have appeared to influence the work reported in this paper.

☐The authors declare the following financial interests/personal relationships which may be considered as potential competing interests: